An ideal terrestrial thermometer using carbonate clumped isotopes from gar scales

Katelyn Gray[ab*] and Mark Brandon[a]

[a] Department of Geology and Geophysics, Yale University, New Haven, CT 06511, United States

[b] Department of Plant & Soil Sciences, University of Delaware, Newark, DE 19716, United States

* Corresponding author at: 221 Academy St, Newark, DE 19716, United States

Keywords: bioapatite, gar, clumped isotopes, paleotemperature

Declaration of Interest: None

Abstract

Carbonate clumped isotope thermometry has been calibrated for a wide variety of carbonates, including calcite, aragonite, dolomite, siderite, and many of their biogenic forms. The clumped isotope composition of the carbonate group substituting for phosphate or hydroxyl in bioapatite ($Ca(PO_4,CO_3)(OH,F)$) has also been temperature calibrated using vertebrate tooth enamel from a range of endothermic body temperatures. We apply this method to other bioapatite-bearing taxa and the calibrated temperature range is extended to lower paleoclimatologically relevant temperatures. Furthermore, because relatively large bioapatite samples are required for carbonate clumped isotope measurements (Δ_{47}), replicate sampling of thin tooth enamel may not be feasible in many situations. Here, we use gar fish (*Lepisosteus sp.*) scales to extend the calibration. These fish are unique in that they are entirely covered in ganoine scales, which are >95% hydroxyapatite. Their enamel structure also makes them resistant to

diagenesis. Additionally, gar fossils are common in lacustrine, fluvial, and near-shore facies, and have a wide distribution in time (Cretaceous to modern) and location (North America, South America, Europe, India, and Africa). We have developed a reliable lab protocol for measuring Δ_{47} in gar bioapatite. We estimate the standard error (SE) for a single measurement as 0.027‰, which is based on replicate analyses and Student T-distribution to account for sample size. We report results for modern gar scales from seven North American localities with mean annual water temperatures (MAWT) ranging from 9 to 26 °C. These data give a temperature calibration curve for gar scales of $\Delta_{47} = (0.1095 \pm 0.0159) \times 10^6/T^2 - (0.5941 \pm 0.0548)$ ($R^2 = 0.74$) and a curve for pooled bioapatite of $\Delta_{47} = (0.1003 \pm 0.0144) \times 10^6/T^2 - (0.4873 \pm 0.0495)$ ($R^2 = 0.76$)

1. Introduction

Paleoclimate studies rely heavily on temperature records, and most records come from marine settings; it is relatively difficult to measure past climatical conditions in terrestrial environments. Commonly used methods include leaf shape analysis (Wilf, 1997; Wolfe and Spicer, 1999), the presence and size of ectotherms (Markwick, 1998; Wing and Greenwood, 1993), and palynology (e.g., Germeraad et al., 1968; Traverse, 2007). A drawback with leaf shape analysis is a lack of understanding of the underlying physiological basis that defines leaf shape. Historical ectotherm ranges are limited by correlating fossil species with modern analogs. Fossil pollen is highly subject to geologic reworking and may only be resolvable to the family or genus level. Branched GDGTs in soils have been used as a temperature proxy, but the empirical MDT-CBT calibration has large errors of 4.8 °C (1 σ), and may be biased by soil pH and aridity (Peterse et al., 2012). These methods are based on empirical correlations with available climate

variables such as surface (as measured at 2 m) air temperature. They are commonly referred to as proxies because they are based on correlations rather than distinct causal processes.

Stable isotopic methods provide a more direct approach to measuring paleotemperature. The oxygen isotope method ($\delta^{18}O$) is the oldest and most widely used, and it has been applied to foraminifera, gastropods, and fish (Grossman and Ku, 1986; Pucéat et al., 2010) and carbonate deposits in soils and adjacent lakes (Leng and Marshall, 2004; Swart, 2015). A challenge is that these estimates require an independent measurement of the ambient water at the time of host mineral formation. Carbonate clumped isotopes is a newer method that provides an estimate for both the temperature and the isotopic composition of the water (e.g., Eiler, 2007; Eiler and Schauble, 2004; Wang et al., 2004). Here we apply this method to bioapatite, which is commonly found in teeth, bones, and fish scales.

Natural settings have large temperature variations, both in time and space. For example, Still et al. (2019) demonstrate via thermal imaging that temperatures on a hill slope at a point in time range from 35 to 70 °C. A long-term record for this hill slope shows that temperatures associated with diurnal and seasonal variations range from 0 to 70 °C. This setting has a low potential for producing a useful paleoclimate record, not only because of the large variation in temperature but also because the highly localized temperatures are not connected in a clear manner to regional climate. A counter example is the isotopic record of benthic foraminifera. In fact, the success of this paleoclimate indicator is largely due to the stable and predictable temperature conditions in the deep ocean.

We contend that gar scales have the potential to provide a long-term average of surface temperature. They therefore have the potential to provide essential climate information for the terrestrial realm in a manner similar to what benthic foraminifera have done for the deep ocean.

Gars have a number of important attributes: (a) they are found in a wide range of terrestrial environments (Lee et al., 1980; Netsch and Witt, 1962) and over a long period of geologic time, (b) individuals have a restricted range and do not migrate (e.g., Buckmeier et al., 2013; Snedden et al., 1999), (c) their scales grow throughout their lifetime, providing a decadal averaged environmental record (e.g., Buckmeier, 2008; Haase, 1969), (d) their scales are highly resistant to diagenesis and commonly occur in the fossil record (Grande, 2010), and (e) the bioapatite in their scales can be analyzed for temperature and isotopic water composition using clumped isotopes.

We present a method to prepare and measure gar scale bioapatite for Δ_{47} that is reproducible at a level comparable to analytical error. These Δ_{47} measurements from scales are compared to temperature along a latitudinal gradient in northern North America to calibrate a paleothermometer. 'Effective temperatures' are calculated using a method from archaeological dating that takes into account seasonal and diurnal variations in surface air temperatures, which are then adjusted to yearly average riverine and lacustrine temperatures. Lastly, we resolve seasonal growth effects using metabolic rate to estimate effective temperatures, with the potential to be relevant to other paleoclimate studies.

1.1. CO_2 clumped-isotope thermometer

The CO_2 clumped-isotope thermometer is based on the concentration of CO_2 molecules with multiply substituted rare isotopes, where ^{13}C and ^{18}O are rare isotopes, and ^{12}C and ^{16}O are common isotopes. The most common doubly-substituted variety of CO_2 is $^{13}C^{18}O^{16}O$, with a mass number of 47. The CO_2 clumped-isotope thermometer compares a sample's concentration of mass 47 CO_2 to its theoretical concentration if the C and O isotopes were randomly distributed

among all mass 47 isotopologues. The ability to accurately measure these isotopologues, which have concentrations in the parts per million, is a recent technological development. Eiler and Schauble (2004) applied this method to measure ^{13}C-^{18}O bond abundance in atmospheric CO_2. Ghosh et al. (2006a) showed that CO_2 extracted by phosphoric acid digestion preserved the isotopologue distribution of the original carbonate anion, CO_3^{2-}, in the host mineral.

The Δ_{47} measurement used in CO_2 clumped-isotope measurements is defined in an idealized fashion by

$$\Delta_{47} = [(R^{47}/R^{47*} - 1) - (R^{46}/R^{46*} - 1) - (R^{45}/R^{45*} - 1)]$$

where R^{47}, R^{46}, and R^{45} are the abundance ratios of masses 47, 46, and 45 relative to 44, and R^{47*}, R^{46*}, and R^{45*} are the stochastic values for this ratios (Affek and Eiler, 2006; Eiler, 2007; Eiler and Schauble, 2004; Wang et al., 2004). In practice, most labs are unable to measure R^{46} and R^{45} (notable exception is Prokhorov et al. (2019)). Fortunately, variations in R^{47} account for most of the multiple substitutions that occur in CO_2 (Schauble et al., 2006). As a result, clumped isotope results are approximated by

$$\Delta_{47} \approx (R^{47}/R^{47*} - 1)$$

where $R_{46} = R_{46*}$ and $R_{45} = R_{45*}$ (see Appendix A in Zaarur et al., 2013, for details). An additional approximation involves the isotopic compositions of C and O in the sample CO_2. $\delta^{13}C$ and $\delta^{18}O$ are measured, but the quantity of ^{17}O is not measured directly, and Δ_{47} must be corrected accordingly for mass interference of ^{17}O. ^{17}O and ^{18}O are related via the relationship (Brand et al., 2010; Gonfiantini et al., 1995)

$$^{17}R = K \cdot (^{18}R)^{\lambda}$$

where K is a coefficient for ^{17}R and ^{18}R in the reference material and λ is a phenomenological constant that links the fractionation that occurs among the different isotopes

of oxygen. By using the λ value of Brand et al. (2010) instead of the original λ value of Gonfiantini et al. (1995), the calculated Δ_{47} was found to be much less sensitive to changes in bulk isotopic composition (Daëron et al., 2016). We use the relevant constant $\lambda = 0.528$ (Brand et al., 2010).

The main advantage of carbonate clumped-isotope thermometry is that temperature can be estimated independent of the isotopic composition of the water and dissolved carbon source. Clumped isotopes have been applied to corals (Saenger et al., 2012; Thiagaraian et al., 2011), mollusks (Henkes et al., 2013), brachiopods (Came et al., 2007), and foraminifera and coccoliths (Tripati et al., 2010). In addition to marine settings, usable carbonates for Δ_{47} can be found in lacustrine settings in the otoliths of fish (Ghosh et al., 2007), terrestrially in the carbonate nodules of fossil soils (Ghosh et al., 2006b), and in the shells of land snails and freshwater gastropods (Zaarur et al., 2011). Carbonate is also found in vertebrate bone, tooth dentin, and enamel, where it occurs in biogenic apatite, primarily in the form of hydroxyapatite, $Ca_5(PO_4)_3(OH)$, with carbonate substituting for the phosphate, PO_4^{3-}, and hydroxyl, OH^-, groups. Carbonate clumped isotope thermometry has been calibrated for bioapatite using modern mammalian and crocodilian teeth (Eagle et al., 2010), modern ostrich bone, African elephant enamel, and shark teeth (Löffler et al., 2019; Wacker et al., 2016).

1.2 Model species, Lepisosteus spp.

Gars belong to the family *Lepisosteidae* and are ancient Actinopterygiians that diverged from crown Teleosts around 342 Ma and have a basal phylogenetic node of 141 Ma (Inoue et al., 2005). They have evolved relatively slowly since this divergence, especially when compared to other vertebrates, including crown Teleosts (Braasch et al., 2016). Today, in North America, gar

fish are found in fluvial and lacustrine settings from Canada to Central America and over into the Caribbean. In the geologic record, they were much more widespread, covering every continent except Australia and Antarctica.

There are seven different living species in *Lepisoteidae*, all of which are found in North and Central America. We focused on the most common species in North America, *Lepisosteus osseus*, which has a distribution that includes drainages in the Mississippi River Valley and the Atlantic margin. When *L. osseus* samples were not available, scales from a sister taxon, *L. platostomus*, the shortnose gar, or *L. oculatus*, the spotted gar, were used instead. The tropical gar, *Atractosteus tropicus*, was selected to represent higher temperature tropical environments. All of these species are capable of hybridization and have similar life histories (Bohn et al., 2017). Any phylogenetic, ecological, or other biological effects on scale isotopic compositions are expected to be similar across taxa.

A significant amount of body mass and length is accumulated within the first year and growth slows to a steady rate after sexual maturity (Netsch and Witt, 1962). Gar grow year-round (e.g., McGrath, 2010; Solomon, 2012), with faster growth in the first three years of life. At that point, longnose gars have a total length of ~650 mm for males and ~730 mm for females (Johnson and Noltie, 1997). For *L. osseus*, scales do not begin to ossify until a standard snout vent length of approximately 150 mm and bioapatite production begins at 200 mm (Thomson and McCune, 1984). Male longnose gars can live up to 17 years (average 8 years) and females can live up to 25 years (average 9 years) (Smylie et al., 2016). Alligator gar are more long-lived, averaging 11 and 14 years for males and females, respectively (Ferrara, 2001). The upper age limit is >60 years (Buckmeier et al., 2012).

An important feature of gar scales for our study is that they grow continuously throughout the gars' adult lives and thus potentially provide a decadal record of surface temperature. The banding in scales is a growth artifact, as it is produced in a manner similar to mammalian enamel (Braasch et al., 2016), which exhibits growth striations on daily and weekly bases (Boyde, 1964; Bromage, 1991; Dean, 1987). The bioapatite is deposited episodically when its base scale reaches a critical size (Thomson and McCune, 1984) and thus scales do not represent seasonal growth cycles.

Gar scales have been used in a small number of paleoclimate studies. Fricke et al. (1998) measured $\delta^{18}O_{phosphate}$ from fossil gar scales along with mammalian teeth from the Eocene of the Bighorn Basin, Wyoming, USA, to predict $\delta^{18}O_{water}$. Fricke and Pearson (2008) measured $\delta^{18}O_{carbonate}$ in gar scales from late Maastrichtian fluvial sediments of North Dakota, USA. The temperature of the Late Eocene fluvial sediment in the UK was estimated using a combination of $\delta^{18}O$ in gar scales, gastropods, otoliths, gyrogonites, and rodent teeth (Grimes et al., 2003). These studies show reproducible measurements and credible temperature estimates.

2. Materials and Methods

2.1 Specimen acquisition

Modern specimens of *Lepisosteus osseus* and *L. platostomus* were acquired either by hook-and-line fishing or through coordination with the Mississippi Wildlife, Fisheries, & Parks Department (Jackson, MS), the Illinois Department of Natural Resources (Springfield, IL), and the Tennessee Wildlife Resources Agency (Nashville, TN), who obtained specimens by gill netting, electrofishing, or collecting by-catch (Table 1 and Figure 1). Where appropriate, individuals were euthanized with an overdose of Tricane methanesulfonate (MS-222), as

indicated in Protocol 2012-10681 approved by Yale University's Institutional Animal and Use Committee (IACUC). Specimens were also received on loan from the University of Michigan Museum of Zoology (UMMZ) collections and the Yale Peabody Museum Collections (YPM), either skeletonized or preserved in ethanol. Only specimens with a standard snout vent length >300 mm to a maximum of 774 mm were sampled to ensure a long record of bioapatite growth.

2.2 Metabolic Rate and effective temperatures

Most paleothermometers are based on empirically-calibrated proxy relationships. For example, the TEX-86 index is calibrated to the mean annual temperature of the overlying sea surface using Archaea in modern ocean sediment cores. The Archaea that synthesize the GDGT compounds used for the TEX-86 index live throughout the water column, and have the highest abundances below the base of the photic zone (>80 m water depth)(Pearson and Ingalls, 2013). Nonetheless, the design of the calibration means that the TEX-86 temperature equation is optimized to predict mean annual sea-surface temperature, even though Archaea live well below the surface.

Isotopic methods are designed, at least in theory, to provide a direct estimate of temperature at the time of precipitation of the host material. More specifically, if one could measure Δ_{47} and calculate temperature at infinitesimal points in a gar scale, a large variation would be expected due to variation in ambient temperature throughout the year. The individual Δ_{47} measurements in our study were determined for a full scale, which means that they were averaged over multiple years.

A key issue is how to relate our Δ_{47} measurements to ambient temperature in a way that avoids the variable temperature associated with diurnal and seasonal variations. To address this

issue, we propose using a method that accounts for variable environmental temperature in the racemization of amino acids and hydration of volcanic glass, which are used as dating methods in archeology and geomorphology (McCoy, 1987; Rogers, 2007). Rogers (2007) proposes a method that accounts for the temperature sensitivity of the chemical reaction associated with glass hydration. His method is built on the idea of estimating an *effective temperature*, which is defined as the steady temperature needed to produce the same amount of hydration as observed in a sample with a variable temperature history.

The effective temperature method requires a specification of the temperature sensitivity of the process. The reaction rates for amino-acid racemization and glass hydration are known to follow an Arrhenius relationship. Gillooly et al. (2001; 2002) and Brown et al. (2004), along with others, have investigated the rates of a wide variety of biological processes, including metabolic rate and growth rate, across a wide range of organisms, including fish. Their universal metabolic equation is

$$B \propto M^{3/4} e^{-Ea/RT}, \quad (1)$$

where B is metabolic rate (kJ s^{-1}), M is body mass (kg), E_a is the activation energy (kJ mol^{-1}), R is Boltzmann's constant (8.314 kJ mol^{-1} K^{-1}), and T is the absolute temperature (K). The Arrhenius relationship for reaction rate as a function of temperature is accounted for by the exponential factor on the right (Boltzman factor). Brown et al. (2004) recommended an average value for E_a = 0.63 eV = 61 kJ/mol. They argue that this value holds for all organisms.

Ecological theory requires that growth rate be proportional to metabolic rate. The equation above shows that warmer temperatures result in faster growth. Thus, our samples will be biased towards the warmer times in their life cycle. The calculation of an effective temperature removes this bias. Because there is little variation in body mass among adult gars,

growth rate for adult gars can be viewed as proportional to the Boltzman factor. As a result, the Rogers (2007) method for calculating effective temperature is directly applicable.

Following Rogers (2007), the time variation in temperature over a year is represented by

$$T(t) = T_{MAT} + \frac{\Delta T_{SR}}{2}\sin(2\pi t) + \frac{\Delta T_{DR}}{2}\sin\left(\frac{2\pi t}{365}\right), \quad (2)$$

where T is temperature (K), t is time (a = annum), T_{MAT} is the mean annual temperature (K), and ΔT_{SR} and ΔT_{DR} are the seasonal and daily ranges in temperature (K). The mass production rate, P, (mass/time) of gar scales is represented by Arrhenius relationship,

$$P = P_0 \exp\left(\frac{E_a}{RT}\right), \quad (3)$$

where P_0 is a pre-exponential constant. The effective temperature, T_{e} is defined by

$$T_e = \int_0^1 P\big(T(t)\big)T(t)dt \Big/ \int_0^1 P\big(T(t)\big)dt, \quad (4)$$

which represents the weighted mean of the temperature, with the weighting provided by P. There is no analytical solution for (4), but the integrations are easily solved numerically (for details, see Rogers, 2007).

Figure 2 shows a comparison of $T_{\mathrm{effective}}$ against T_{MAT} for 19,874 North America stations (excluding Greenland) for the time interval from 1900 to 2018 (surface air temperature at 2 m height above ground provided by the Global Historical Climatology Network (GHCN) database Menne et al. (2012)). These data were used to calculate mean values for T_{AM}, ΔT_{SR}, and ΔT_{DR} at each station. The stations provided an average record length of 11 years for these estimates due to partial records. Note that T_{e} is always greater than T_{MAT} by as much as 12 °C. This difference increases with decreasing temperature, which is consistent with the fact that surface air temperature is most steady in the tropics and most variable in the polar regions, and the production rate P increases with increasing temperature.

For our gar calibration, $T_{\mathrm{AM},}$ ΔT_{SR}, and ΔT_{DR} were estimated for each sample site using the 1-km gridded Daymet dataset (Thornton et al., 2017; Thornton et al., 1997). Daymet was constructed using a truncated Gaussian filter to approximately 11,000 stations under the National Weather Service Cooperative Observer Program (NWS COOP), weighting stations by distance from an arbitrary point. Predicted temperatures were estimated using a weighted least-squares regression. We added 1 °C to Daymet temperatures to account for the positive offset of river water temperature relative to air temperature (Fricke and Wing, 2004).

2.3 Specimen pretreatment

Approximately 5 cm x 5 cm sections of scales were taken from the left lateral side of the fish, as the alternative side is commonly left for archival purposes, and given to dermestid beetles for several days to remove collagen and other organic tissues (Hefti et al., 1980). Debrided scales were further cleaned by scalpel and tweezers. Approximately 1 g of scales from each specimen were cryogenically milled in a 6750 Freezer/Mill (SPEX CertiPrep) for 3 minutes.

Unlike the bioapatite used in Wacker et al. (2016) and Eagle et al. (2010), gar scales have an initial higher concentration of organic matter. We sampled whole scales, including the enamel layer and the underlying bone, as it is difficult to distinguish between the two with the naked eye. Both are assumed to have the same initial isotopic composition. The mineralized bone is interwoven with collagen, and the enamel is covered by collagen during life. They are pitted with vertical canals that contain miniature blood vessels and mesoderm cells (Kerr, 1952). Gar scales interlock and are further connected *in vivo* by the fibrous collagen of the stratum compactum (Gemballa and Bartsch, 2002). Gar scales share the same XRD peaks as carbonate

hydroxyapatite (LeGeros and Suga, 1980; LeGeros et al., 1967) but have high initial contents of 9.4 ± 0.8% organic carbon and 3.24 ± 0.3 nitrogen (Supplemental Table 1), which is related to the organic material that these scales possess *in vivo*.

Some of the organic material can be mechanically removed, but chemical treatment of samples was needed for complete removal. Any stray hydroxyl groups on the collagen matrix, such as from glycine, proline, and hydroxyproline (Eastoe, 1957) which surround the ganoine scales, likely react with the acid during digestion, producing water, as detected by elevated mass 18 values. For a detailed discussion of the effect of chemical treatment methods on gar scale clumped isotopic values, see Gray (2018).

Koch et al. (1997) found that treatment with 30% H_2O_2 did not affect the isotopic values of enamel hydroxyapatite. Milled samples were sonicated (Sonicor DSC-100TH) for several hours with 30% H_2O_2 to remove organic carbon. Scales were considered clean when bubbling from the reaction ceased. Scales were then rinsed with DI water, agitated, and centrifuged; this process was repeated six times. Samples were dried in a vacuum (Isotemp Vacuum Oven Model 280A, Fisher Scientific, USA) at 40 °C for two days. XRD showed an increase in bioapatite peaks after sonication, particularly at the [002] and [211] peaks, 25.9° and 31.8° 2Θ, respectively.

2.4 Acid digestion and Δ_{47} Measurement

Wacker et al. (2013) noted a sample size effect on Δ_{47} when carbonate samples <7 mg were digested at 25 °C. Wacker et al. (2016) found a similar effect for bioapatite from elephant tooth enamel. They inferred that at the lower reaction temperature, there was partial re-equilibration of the resultant gas with water. Wacker et al. (2016) increased the reaction

297 temperature to 110 °C for bioapatite to decrease the reaction time. They noted that the partial
298 pressure of the water vapor above the acid was four times greater, which is much larger than
299 expected for a 20 °C increase in temperature. Water is known to adversely affect bond ordering
300 in CO_2 samples. Our choice of a 90 °C instead of a 25 °C reaction temperature was meant to
301 avoid this problem. It is also more consistent with the reaction temperature used in most clumped
302 isotope labs.

303 Samples ranging from 45 to 55 mg were reacted in an isolated McCrea vessel with 105%
304 H_3PO_4 (ρ = 1.93 g/cm^3) at 90 °C. Reactions lasted for 20 to 40 minutes and were considered
305 complete when visible bubbles stopped forming. Because modern material has a large organic
306 component and the $-OH^-$ group from the bioapatite scale reacts with the H^+ ions in the acid to
307 form water, extra care was taken to purify the extracted CO_2 on a Pyrex vacuum line. For every
308 torr of CO_2 produced from the acid digestion, about 1 to 1.5 torr of water was also produced. To
309 avert re-equilibration with water, samples were kept under constant vacuum throughout the
310 reaction and were continuously collected. Water was removed by forcing the sample twice
311 through an ethanol-liquid nitrogen trap held at less than -85 °C. Sample CO_2 was then passed
312 through silver wool to remove any sulfur compounds (Eiler, 2007).

313 Purified CO_2 was then passed through a homemade stainless-steel column (1.22 m long x
314 0.3175 cm OD) filled with Poropak Q 50-80 mesh (Waters Technologies Co., USA) and housed
315 in a gas chromatograph (Varian CP-3800, USA). This step was to ensure that sample CO_2 had no
316 remaining hydrocarbons or halocarbon contaminants, which can interfere with the mass 47
317 measurement (Eiler and Schauble, 2004). The Poropak Q was ultimately chosen over Supelco Q-
318 Plot due to its better ability to handle organic rich samples.

During chromatography, samples were held at a constant -20 °C and carried with helium at a rate of 5 mL/min for approximately 45 minutes through the column. CO_2 was frozen cryogenically after being forced through the GC column and passed through the water trap two more times before being placed on the mass spectrometer. The GC column was baked at 150 °C between each sample run. After every four samples, or once daily, it was baked at 220 °C for 600 minutes (Huntington et al., 2009).

Measurements were performed on a MAT 253 dual-inlet gas-source isotope ratio mass spectrometer (ThermoFisher Scientific, USA) housed at the Yale University Analytical and Stable Isotope Center. The MAT 253 was modified to measure masses 44 through 49 simultaneously in dual-inlet mode, alternating between sample gas and reference gas. The standard three Faraday cups were used to measure masses 44, 45, and 46, with an additional three cups to measure masses 47, 48, and 49, with the same currents and resistances as Eiler and Schauble (2004). Further modifications were made to the Yale mass spectrometer to allow measurement of small samples (Zaarur et al., 2011). Measurement routines were as outlined by Huntington et al. (2009) and Zaarur et al. (2011): nine acquisitions of 10 cycles each with eight seconds of integration time for the reference and sample gas each cycle. There were two additional acquisitions of two cycles each to measure the background voltage. Bulk oxygen and carbon isotopic compositions were made using Oztech Trading Co. CO_2 (Safford, AZ) as a working standard, with a composition of $\delta^{18}O$ = -3.629 ‰ and $\delta^{13}C$ = 24.992 ‰, which allowed for conversion to the VSMOW scale.

Measurements of Δ_{47} were calculated based on the excess of mass 47 from a stochastic distribution of isotopologues with varying bulk carbon and oxygen isotopic compositions. The stochastic distribution was determined by heating pure CO_2, with a wide range of $\delta^{18}O$ and $\delta^{13}C$

compositions, to 1000 °C for two hours to reset its Δ_{47} value (Eiler and Schauble, 2004). These heated gases were run on a weekly basis, or about every 10 to 15 samples. To correct for scale compression, which varies with time in a single lab and between labs, CO_2 was equilibrated with water at 25 °C (Affek, 2013; Dennis et al., 2011). Carrara marble was regularly run as an internal carbonate standard, as well as cylinder CO_2 (Airgas, USA).

To fit data into an absolute reference frame (Dennis et al., 2011), data were adjusted using an empirical transfer function slope that averages changes in the heated gas line over time. Prior clumped isotope work had used ^{17}O abundance correction values from Gonfiantini et al. (1995), but their recommended λ of 0.5164 – the relationship between $\delta^{17}O$ and $\delta^{18}O$ – was based on a study that used a combination of waters and rocks to estimate the coefficient (Matsuhisa et al., 1978). Brand et al. (2010) recommended $\lambda = 0.528$ as a better representation of the terrestrial fractionation of surface waters. Additionally, the choice of this λ value, along with the R^{17} and R^{18} values as reported in Brand et al. (2010), appear to make Δ_{47} measurements truly independent of the bulk isotopic composition (Daëron et al., 2016). Raw Δ_{47} were converted using the Brand et al. (2010) parameters as outlined in Daëron et al. (2016).

3. Results

3.1 Temperature dependence of Δ_{47} and independence from bulk composition

The lack of correlation between the clumped isotopic measurement (Δ_{47}) and the isotopic bulk composition ($\delta^{18}O_{carbonate}$ and $\delta^{13}C_{carbonate}$, hereafter labeled $\delta^{18}O_c$ and $\delta^{13}C$) suggested that they were independent (Figures 3 and 4). $\delta^{13}C$ was assumed to be mostly influenced by diet. The range of $\delta^{13}C$ values was consistent with the fact that gars are predators, or secondary consumers (Fricke and Pearson, 2008; Gu et al., 1996). In addition, factors other than temperature and

$\delta^{18}O_{water}$ may influence the $\delta^{18}O_c$ – temperature relationship in modern fishes, such as the specific placement of the carbonate ion in the bioapatite lattice (Kolodny and Luz, 1991).

The lowest Δ_{47} values obtained from gar scales were 0.657 to 0.664‰ from *A. tropicus* specimens from Mexico, and the highest Δ_{47} values were 0.718 to 0.810‰ from *L. osseus* specimens from Michigan, USA. A least squares linear regression of the inverse squared effective temperature experienced by gars versus Δ_{47} values produced a calibration line

$$\Delta_{47} = (0.1095 \pm 0.0159) \times 10^6 / T^2 - (0.5941 \pm 0.0548), \quad (5)$$

with $R^2 = 0.7358$ (Figure 5).

A second calibration line was calculated that included elephant tooth enamel as a high temperature endmember (T = 36.2 °C; Δ_{47} = 0.582‰; temperature from Kinahan et al. (2007)). Sand tiger shark dentine was not added because its bulk isotopic composition is different from its overlying enameloid (Löffler et al., 2019). The fluoride-rich quality of shark bioapatite sets it apart from the other sampled species in the bioapatite calibration. The enameloid of the Greenland shark (Löffler et al., 2019; Wacker et al., 2016) was not included because its growth temperature was not well constrained. These sharks migrate from higher latitudes with temperatures ~ -2 °C to lower latitudes with water temperatures as warm as 10 °C (MacNeil et al., 2012), and they are found from just below the surface to >1200 m depths (Yano et al., 2007). The Greenland shark of Wacker et al. (2016) and Löffler et al. (2019) was recovered off of the coast of Iceland, which is at the crossroads of several major currents with different salinities, temperatures, and oxygen isotopic compositions. Temperatures of 7.0 °C are obtained when the appropriate phosphate-oxygen thermometer (Pucéat et al., 2010) is used to estimate its temperature. Additionally, the effective temperature of a Greenland shark that on average

387 experiences temperatures of 2 °C is 4 °C; for 5 °C, it is 7 °C. The bioapatite from Eagle et al.
388 (2010) were not included as they correct ^{17}O with the Gonfiantini et al. (1995) λ.

389 The combined calibration of T vs Δ_{47} for bioapatite from gars *in vivo* and for endotherms
390 that produce true enamel, with known internal body temperature, produce the calibration

391 $$\Delta_{47} = (0.0987 \pm 0.0140) \times 10^6/T^2 - (0.4658 \pm 0.0481) \quad (6)$$

392 with $R^2 = 0.798$ (Figure 6).

393 The Δ_{47} values from gar scales are skewed high compared to the synthetic apatite of
394 Löffler et al. (2019). Equation (6) for all bioapatite is more robust due to its $X^2 = 1.410$ versus X^2
395 = 2.790 for the calibration from gar scales alone in Equation (5). A clear offset is recognized at
396 colder temperatures (<15 °C MAT).

397

398 **4. Discussion**

399 *4.1. Comparison to other calibrations*

400 The clumped isotope community is often troubled by the lack of consistency among lab
401 calibrations, but recent modifications to their development have helped minimize these
402 discrepancies. This was first addressed in Dennis et al. (2011), who developed an absolute
403 reference frame established on the projection of Δ_{47} measurements onto an "absolute scale"
404 based on theoretical predictions about the equilibrium relationship of Δ_{47} as a function of
405 temperature (Wang et al., 2004). The absolute reference frame provides support for inter-
406 laboratory reproducibility to a level of 0.017 and 0.008‰ (1 σ). The heated gas intercept was
407 also recalibrated to account for the scrambling (the fragmentation and recombination reactions of
408 the sample CO_2) within the ion source of a mass spectrometer.

There remains some discordance between labs, which some have attributed to differences in the reaction temperature used for the phosphoric-acid step. It is well known that there is a temperature-dependent isotopic fraction of CO_2 gas produced by phosphoric-acid dissolution of carbonate. The acid fractionation factor between reactions at 25 °C and 90 °C was re-measured by Henkes et al. (2013) as 0.076‰ ± 0.007‰, which is within 1 σ error to the original value.

Kelson et al. (2017) set to create a universal calibration using different methods of synthesizing carbonates over a wide range of temperatures and added these results to the current pool of Δ_{47} measurements. The scatter between calibrations decreases with the use of the Brand et al. (2010) parameters (Kelson et al., 2017).

A clumped isotope calibration using unvarying isotopically very heavy or very light bulk composition carbonate with the Gonfiantini et al. (1995) parameter may be noticeably different from a calibration that does not. Zaarur et al. (2013) created isotopically very light $\delta^{13}C$ carbonate—from -35.09‰ to -17.53‰—compared to other synthetic calibrations. Holding the acid digestion temperature constant, it has a steeper slope, even after correction with Brand et al. (2010). Kelson et al. (2017) explains the main calibration discrepancy as perhaps arising from lab differences in isolating the CO_2 before isotopic measurement. Lab standards were reproducible among the setup used by Zaarur et al. (2013) and others, so this is likely not the cause (Dennis et al., 2011; Henkes et al., 2013). It may be biased because the starting bulk composition of the synthetic carbonate is lighter from that used in other labs, as they are generally -20 ‰ or heavier. It likely does not fall on the terrestrial meteoric water line.

When the samples in this study were modified using the ^{17}O correction parameters of Brand et al. (2010) as exemplified in Daëron et al. (2016), the slope was not affected, only the intercept, in similar fashion to other ^{17}O corrected synthetic carbonate calibrations (Kelson et al.,

2017). If the bulk composition truly affects the calibration due to the choice of ^{17}O parameters, the range of $\delta^{13}C$ from this study, from -5.29‰ to -9.47‰, should have minimal effects, since they are not on either extreme: isotopically very enriched or very depleted.

The laboratory set-up used here with a GC column of Poropak Q and constant CO_2 entrapment during the reaction is similar to several labs, but it does not account for the significantly steeper slope seen in bioapatite. Additionally, the in-house standard YCM was run at 25 °C and 90 °C through a Supelco Q-Plot column and through a Poropak Q column within a GC. No significant difference was seen in Δ_{47} among the disparate cleaning methods. Only the acid digestion temperature had an effect, which was expected. The in-house clumped isotope standard, Yale Carrara Marble (YCM), has a long-term running average of $\Delta_{47abs} = 0.418 \pm 0.016$ (1 σ) at 25 °C. At 90 °C, $\Delta_{47abs} = 0.357 \pm 0.015$ (1 σ), an offset within error to the acid fractionation factor $\alpha_{25\text{-}90} = 1.0076 \pm 0.007$ (Henkes et al., 2013).

4.2 Biological explanations for discrepancy

The enamel scales of gar are produced by proteins encoded by the genes *ambn* and *enam*, which are also present in lobe-finned vertebrates, including mammals (Braasch et al., 2016). When carbonate is incorporated into bioapatite, it either takes the place of hydroxyl (A-type substitution) or phosphate (B-type substitution), with the latter placement 28% more prevalent in mammalian bone (Rey et al., 1989).

The fractionation factor between inorganic phosphate (and consequently carbonate) and bioapatite in mammals is species dependent or at least affected by a combination of genetic and lifestyle influences (Ayliffe and Chivas, 1990; D'Angela and Longinelli, 1990; Longinelli, 1984). Gar likely follow a calibration curve similar to mammals, but a mammalian-only calibration

curve is not feasible because mammals maintain a constant 37 °C body temperature regardless of phylogenetic placement.

The potential of isotopic mixing as postulated by Henkes et al. (2013) for mollusks should not apply for gar; the mollusks were time averaged over a year, whereas these fish are averaged over several years to decades. Even if isotopic mixing affected the calibration curve, Henkes et al. (2013) estimated that the effect it would have on the mollusk curve would be minimal.

Incorporation of carbon from dissolved inorganic carbon (DIC) from dietary sources has been observed in shark teeth (Vennemann et al., 2001). This DIC has a residual low Δ_{47} signal when incorporated into body tissues, which only becomes an issue if the DIC was diffused from the environment. The one correlation that may indicate kinetic isotope effects, $\delta^{18}O_{carbonate}$, shows no relationship to Δ_{47}. No enrichment in measured $\delta^{18}O_{carbonate}$ over expected values is seen for samples. There is also no correlation between Δ_{47} and $\delta^{13}C$ (Figure 4 B).

4.3 Benefits of natural calibrations

Laboratory experiments can only partially recreate complex isotopic systems. Watkins et al. (2014) found that non-equilibrium isotopic effects from inorganic calcite precipitation can produce up to a 2‰ $\delta^{18}O$ offset. The universal calibration of Kelson et al. (2017) may be true for inorganic calcite, but there are other confounding variables, especially those affiliated with biogenic mineral precipitation (e.g., Henkes et al., 2013; Saenger et al., 2012; Thiagaraian et al., 2011; Zaarur et al., 2011). Hidden variables due to biology or other factors are accounted for when using a natural calibration on natural samples. In this regard, the Δ_{47} of bioapatite samples, including fossils, should not be converted to temperature using a purely carbonate calibration.

5. Conclusions

The clumped isotopic composition of bioapatite from multiple sources, including gar scales, produces a real temperature signal that is different from the Δ_{47}-T relationship for carbonates, most notably at low temperatures. This divergence cannot be attributed to laboratory differences or disparity in data transformation and therefore likely represents a unique relationship possessed by vertebrates. Its steeper slope makes it more sensitive to temperature changes, further increasing its utility on land.

Ganoine is found not only in gar scales but also in the scales of closely related species, such as the living Polypteriformes and fossil Semionotiformes. Assuming a similar Δ_{47}-T relationship occurs for these ancient fish, terrestrial temperatures could be estimated as far back as the Triassic. Today, gar are commonly seen as 'trash fish,' as they can inhabit low-quality water and their tough exterior makes them largely inedible. This fundamental survivorship quality, along with paleontologists' relative apathy toward them, gives gar and their affiliated isolated scales great potential to reconstruct past terrestrial climates.

Furthermore, the independent temperature proxy, Δ_{47}, can be coupled with $\delta^{18}O_{carbonate}$ from the same single clumped isotope measurement to infer $\delta^{18}O_{water}$. The $\delta^{18}O_{carbonate}$ value could be replaced with one from $\delta^{18}O_{phosphate}$, as it provides a more robust signal. The $\delta^{18}O_{water}$ values from a single measurement offer insight into the hydrological cycle. When applied to fossil samples from terrestrial paleoenvironments across a region or across time, these values can indicate changes in the cycle.

Gar scales are abundant in the fossil record. Two of the most concentrated localities where gar scales are found are the Green River Formation of Wyoming and the Messel

Formation in Germany (Grande, 2010), both of which formed during the Eocene period. While the greatest concentrations of gar fossils are from North America and Europe, there are also notable fossil deposits from the Cretaceous of Morocco and Brazil. All of these deposits are inferred to be fluvial or lacustrine in origin and represent glimpses into terrestrial environments.

Acknowledgements

This research was partially funded through a Yale Institute for Biospheric Studies grant to K.E. Gray. Deepest gratitude goes to the late Mark Pagani for his ideas and insight into this project. All measurements were done at the Yale Analytical and Stable Isotope Center (YASIC). Greg Watkins-Colwell of the Yale Peabody Museum assisted in gar scale removal and cleaning. Douglas Nelson, Fishes Collection Manager at the Museum of Zoology at the University of Michigan greatly assisted in providing specimens to sample. Other acquired specimens were obtained with help of the Mississippi Department of Wildlife, Fisheries, and Parks; the Tennessee Wildlife Resources Agency; and the Illinois Department of Natural Resources.

References

Affek, H.P. (2013) Clumped Isotope Equilibrium and the Rate of Isotope Exchange Between CO_2 and Water. American Journal of Science 313, 309-325.

Affek, H.P. and Eiler, J.M. (2006) Abundance of mass-47 of CO_2 in urban air, car exhaust, and human breath. Geochimica et Cosmochimica Acta 70, 1-12.

Ayliffe, L.K. and Chivas, A.R. (1990) Oxygen isotope composition of bone phosphate of Australian kangaroos: Potential as a paleoenvironmental recorder. Geochimica et Cosmochimica Acta 54, 2603-2609.

Bohn, S., Kreiser, B.R. and Bodine, K.A. (2017) Natural Hybridization of Lepisosteids: Implications for Managing the Alligator Gar. North American Journal of Fisheries Management 37, 405-413.

Boyde, A. (1964) The Structure and Development of Mammalian Enamel, Department of Anatomy. University of London, London.

Braasch, I., Gehrke, A.R., Smith, J.J., Kawasaki, K., Manousaki, T., Pasquier, J., Amores, A., Desvignes, T., Batzel, P., Catchen, J., Berlin, A.M., Campbell, M.S., Barrell, D., Martin, K.J., Mulley, J.F., Ravi, V., Lee, A.P., Nakamura, T., Chalopin, D., Fan, S., Wcisel, D., Cañestro, C., Sydes, J., Beaudry, F.E.G., Sun, Y., Hertel, J., Beam, M.J., Fasold, M., Ishiyama, M., Johnson, J., Kehr, S., Lara, M., Letaw, J.H., Litman, G.W., Litman, R.T., Mikami, M., Ota, T., Saha, N.R., Williams, L., Stadler, P.F., Wang, H., Taylor, J.S., Fontenot, Q., Ferrara, A., Searle, S.M.J., Aken, B., Yandell, M., Schneider, I., Yoder, J.A., Volff, J.-N., Meyer, A., Amemiya, C.T., Venkatesh, B., Holland, P.W.H., Guiguen, Y., Bobe, J., Shubin, N.H., Di

Palma, F., Alföldi, J., Lindblad-Toh, K. and Postlethwait, J.H. (2016) The spotted gar genome illuminates vertebrate evolution and facilitates human-teleost comparisons. Nature Genetics 48, 427-437.
Brand, W.A., Assonov, S.S. and Coplen, T.B. (2010) Correction for the ^{17}O interference in d(^{13}C) measurements when analyzing CO_2 with stable isotope mass spectrometry (IUPAC Technical Report). Pure Appl. Chem. 82, 1719-1733.
Bromage, T.G. (1991) Enamel incremental periodicity in the Pig-Tailed Macaque: A Polychrome Fluorescent Labeling Study of Dental Hard Tissues. American Journal of Physical Anthropology 86, 205-214.
Brown, J.H., Gillooly, J.F., Allen, A.P., Savage, V.M. and West, G.B. (2004) Toward a metabolic theory of ecology. Ecology 85, 1771-1789.
Buckmeier, D.L. (2008) Life History and Status of Alligator Gar Atractosteus spatula, with Recommendations for Management, in: TPWD Inland Fisheries Report, H.o.t.H.F.S.C. (Ed.).
Buckmeier, D.L., Smith, N.G. and Daugherty, D.J. (2013) Alligator Gar Movement and Microhabitat Use in the Lower Trinity River, Texas. Transactions of the American Fisheries Society 142, 1025-1035.
Buckmeier, D.L., Smith, N.G. and Reeves, K.S. (2012) Utility of Alligator Gar Age Estimates from Otoliths, Pectoral Fin Rays, and Scales. Transactions of the American Fisheries Society 141, 1510-1519.
Came, R.E., Eiler, J.M., Veizer, J., Azmy, K., Brand, U. and Weidman, C.R. (2007) Coupling of surface temperatures and atmospheric CO_2 concentrations during the Paleozoic era. Nature 449, 198-201.
D'Angela, D. and Longinelli, A. (1990) Oxygen isotopes in living mammal's bone phosphate: Further results. Chemical Geology 86, 75-82.
Daëron, M., Blamart, D., Peral, M. and Affek, H. (2016) Absolute isotoic abunance ratios and the accuracy of Δ_{47} measurements. Chemical Geology 441, 83-96.
Dean, M.C. (1987) Growth layers and incremental markings in hard tissues; a review of the literature and some preliminary observations about enamel structure in *Paranthropus boisei*. Journal of Human Evolution 16, 157-172.
Dennis, K.J., Affek, H.P., Passey, B.H., Schrag, D.P. and Eiler, J.M. (2011) Defining an absolute reference frame for 'clumped' isotope studies of CO2. Geochimica et Cosmochimica Acta 75, 7117-7131.
Eagle, R.A., Schauble, E.A., Tripati, A.K., Tütken, T., Hulbert, R.C. and Eiler, J.M. (2010) Body temperatures of modern and extinct vertebrates from ^{13}C-^{18}O bond abundances in bioapatite. Proceedings of the National Academy of Science 107, 10377–10382.
Eastoe, J.E. (1957) The Amino Acid Composition of Fish Collagen and Gelatin. Biochemical Journal 65, 363-368.
Eiler, J.M. (2007) "Clumped-isotope" geochemistry - the study of naturally-occurring, multiply-substituted isotopologues. Earth and Planetary Science Letters 262, 309-327.
Eiler, J.M. and Schauble, E.A. (2004) $^{18}O^{13}C^{16}O$ in Earth's atmosphere. Geochimica et Cosmochimica Acta 68, 4767-4777.
Ferrara, A.M. (2001) Life history strategy of Lepisosteidae: Implications for the conservation and management of Alligator gar, Fisheries and Allied Aquacultures. Auburn University, Auburn, Alabama, p. 145.
Fricke, H.C., Clyde, W.C., O'Neil, J.R. and Gingerich, P. (1998) Evidence for rapid climate change in North America during the latest Paleocene thermal maximum: oxygen isotope compositions of biogenic phosphate from the Bighorn Basin (Wyoming). Earth and Planetary Science Letters 160, 193-208.
Fricke, H.C. and Pearson, D.A. (2008) Stable isotope evidence for changes in dietary niche partitioning among hadrosaurian and ceratopsian dinosaurs of the Hell Creek Formation, North Dakota. Paleobiology 34, 534-552.
Fricke, H.C. and Wing, S.L. (2004) Oxygen isotope and paleobotanical estimates of temperature and $\delta^{18}O$ latitude gradients over North American in Eocene. American Journal of Science 304, 612-635.
Gemballa, S. and Bartsch, P. (2002) Architecture of the integument in lower Teleostomes: functional morphology and evolutionary implications. Journal of Morphology 253, 290-309.
Germeraad, J.H., Hopping, C.A. and Muller, J. (1968) Palynology of Tertiary Sediments from Tropical Areas. Review of Palaeobotany and Palynology 6, 189 - 348.
Ghosh, P., Adkins, J., Affek, H.P., Balta, B., Guo, W., Schauble, E.A., Schrag, D. and Eiler, J.M. (2006a) 13C-18O bonds in carbonate minerals: A new kind of paleothermometer. Geochimica et Cosmochimica Acta 70, 1439-1456.
Ghosh, P., Eiler, J., Campana, S.E. and Feeney, R.F. (2007) Calibration of the carbonate 'clumped isotope' paleothermometer for otoliths. Geochimica et Cosmochimica Acta 71, 2736-2744.
Ghosh, P., Garzione, C.N. and Eiler, J.M. (2006b) Rapid Uplift of the Altiplano revealed through ^{13}C-^{18}O bonds in paleosol carbonates. Science 311, 511-515.

589 Gillooly, J.F., Brown, J.H., West, G.B., Savage, V.M. and Charnov, E.L. (2001) Effects of Size and Temperature on
590 Metabolic Rate. Science 293, 2248-2251.
591 Gillooly, J.F., Charnov, E.L., West, G.B., Savage, V.M. and Brown, J.H. (2002) Effects of size and temperature on
592 developmental time. Nature 417, 70-73.
593 Gonfiantini, Stichler and Rozanski (1995) IAEA-TECDOC-825, International Atomic Energy Agency, Vienna, pp.
594 13-29.
595 Grande, L. (2010) An empirical synthetic pattern study of gars (Lepisosteiformes) and closely related species, based
596 mostly on skeletal anatomy. The resurrection of Holostei. American Society of Ichthyologists and
597 Herpetologists.
598 Gray, K. (2018) Reconstructing Terrestrial Climates using Clumped Isotope Thermometry and Phosphate Oxygen
599 Isotopes from Gar Scales, Geology and Geophysics. Yale University, New Haven, CT, p. 158.
600 Grimes, S.T., Mattey, D.P., Hooker, J.J. and Collinson, M.E. (2003) Paleogene paleoclimate reconstruction using
601 oxygen isotopes from land and freshwater organisms: the use of multiple proxies. Geochimica et
602 Cosmochimica Acta 67, 4033-4047.
603 Grossman, E.L. and Ku, T.-L. (1986) Oxygen and carbon isotope fractionation in biogenic aragonite: temperature
604 effects. Chemical Geology 59, 59-74.
605 Gu, B., Schelske, C.L. and Hoyer, M.V. (1996) Stable isotopes of carbon and nitrogen as indicators of diet and
606 tropic structure of the fish community in a shallow hypereutrophic lake. Journal of Fish Biology 49, 1233-
607 1243.
608 Haase, B.L. (1969) An ecological life history of the longnose gar, Lepisosteus osseus (Linnaeus), in Lake Mendota
609 and in several other lakes of southern Wisconsin, Zoology. University of Wisconsin, p. 225.
610 Hefti, E., Trechsel, U., Rüfenacht, H. and Fleisch, H. (1980) Use of dermestid beetles for cleaning bones. Calcified
611 Tissue International 31, 45-47.
612 Henkes, G.A., Passey, B.H., Wanamaker Jr., A.D., Grossman, E.L., Ambrose Jr., W.G. and Carroll, M.L. (2013)
613 Carbonate clumped isotope compositions of modern marine mollusk and brachiopod shells. Geochimica et
614 Cosmochimica Acta 106, 307-325.
615 Huntington, K.W., Eiler, J.M., Affek, H.P., Guo, W., Bonifacie, M., Yeung, L.Y., Thiagarajan, N., Passey, B.H.,
616 Tripati, A.K., Daëron, M. and Came, R. (2009) Methods and limitations of 'clumped' CO_2 isotope (Δ_{47})
617 analysis by gas-source isotope ratio mass spectrometry. Journal of Mass Spectrometry 44, 1318-1329.
618 Inoue, J.G., Miya, M., Venkatesh, B. and Nishida, M. (2005) The mitochondrial genome of Indonesian coelacanth
619 Latimeria mendadoensis (Sarcopterygii: Coelanthiformes) and divergence time estimation between the two
620 coelacanths. Gene 349, 227-235.
621 Johnson, B.L. and Noltie, D.B. (1997) Demography, growth, and reproductive allocation in stream-spawning
622 Longnose gar. Transactions of the American Fisheries Society 126, 438-466.
623 Kelson, J.R., Huntington, K.W., Schauer, A.J., Saenger, C. and Lecher, A.R. (2017) Toward a universal carbonate
624 clumped isotope calibration: Diverse synthesis and preparatory methods suggest a single temperature
625 relationship. Geochimica et Cosmochimica Acta 197, 104-131.
626 Kerr, T. (1952) The scales of primitive living actinopterygians. Proceedings of the Zoological Society of London
627 122.
628 Kinahan, A.A., Inge-moller, R., Bateman, P.W., Kotze, A. and Scantlebury, M. (2007) Body temperature daily
629 rhythm adaptations in African savanna elephants (*Loxodonta africana*). Physiology & Behavior 92, 560-
630 565.
631 Koch, P.L., Tuross, N. and Fogel, M. (1997) The Effects of Sample Treatment and Diagenesis on the Isotopic
632 Integrity of Carbonate in Biogenic Hydroxylapatite. Journal of Archaeological Science 24, 417-429.
633 Kolodny, Y. and Luz, B. (1991) Oxygen isotopes in phosphates of fossil fish - Devonian to Recent, in: H.P. Tayor,
634 H.P., O'Neil, J.R., Kaplan, I.R. (Eds.), Stable Isotope Geochemistry: A Tribute to Samuel Epstein.
635 Geochemical Society Special Publications, pp. 105-119.
636 Lee, D.S., Gilbert, C.R., Hocutt, C.H., Jenkins, R.E., McAllister, D.E. and Stauffer, J., Jay R. (1980) Atlas of North
637 American freshwater fishes. North Carolina State Museum of Natural Sciences, Raleigh, NC.
638 LeGeros, R.Z. and Suga, S. (1980) Crystallographic Nature of Fluoride in Enameloids of Fish. Calcified Tissue
639 International 32, 169-174.
640 LeGeros, R.Z., Trautz, O.R., LeGeros, J.P., Klein, E. and Shirra, W.P. (1967) Apatite Crystallites: Effects of
641 Carbonate on Morphology. Science 155, 1409-1411.
642 Leng, M.J. and Marshall, J.D. (2004) Palaeoclimate interpretation of stable isotope data from lake sediment
643 archives. Quaternary Science Reviews 23, 811-831.

Löffler, N., Fiebig, J., Mulch, A., Tütken, T., Schmidt, B.C., Bajnai, D., Conrad, A.C., Wacker, U. and Böttcher, M.E. (2019) Refining the temperature dependence of the oxygen and clumped isotopic compositions of structurally bound carbonate in apatite. Geochimica et Cosmochimica Acta 253, 19-38.
Longinelli, A. (1984) Oxygen isotopes in mammal bone phosphate: A new tool for paleohydrological and paleoclimatological research? Geochimica et Cosmochimica Acta 48, 385-390.
MacNeil, M.A., MacMeans, B.C., Hussey, N.E., Vecsei, P., Svavarsson, J., Kovacs, K.M., Lydersen, C., Treble, M.A., Skomal, G.B., Ramsey, M. and Fisk, A.T. (2012) Biology of the Greenland Shark Somniosus microcephalus. Journal of Fish Biology 80, 991-1018.
Markwick, P.J. (1998) Fossil crocodilians as indicators of Late Cretaceous and Cenozoic climates: implications for using palaeontological data in reconstructing palaeoclimate. Palaeogeography, Palaeoclimatology, Palaeoecology 137, 205-271.
Matsuhisa, Y., Goldsmith, J.R. and Clayton, R.N. (1978) Mechanisms of hydrothermal crystallization of quartz at 250 °C and 15 kbar. Geochimica et Cosmochimica Acta 42, 173-182.
McCoy, W.D. (1987) The precision of amino acid geochronology and paleothermometry. Quaternary Science Reviews 6, 43-54.
McGrath, P. (2010) The Life History of Longnose Gar, *Lepisosteus osseus*, an Apex Predator in the Tidal Waters of Virginia, School of Marine Science. The College of William and Mary, p. 177.
Menne, M.J., Durre, I., Vose, R.S., Gleason, B.E. and Houston, T.G. (2012) An overview of the Global Historical Climatology Network-Daily Database. Journal of Atmospheric and Oceanic Technology 29, 897-910.
Netsch, N. and Witt, A. (1962) Contributions to the Life History of the Longnose Gar, (*Lepisosteus osseus*) in Missouri. Transactions of the American Fisheries Society 91, 251-262.
Pearson, A. and Ingalls, A.E. (2013) Assessing the use of archaeal lipids as marine environmental proxies. Annual Review of Earth and Planetary Science 41, 359-384.
Peterse, F., van der Meer, J., Schouten, S., Weijers, J.W.H., Fierer, N., Jackson, R.B., Kim, J.-H. and Damsté, S.J.S. (2012) Revised calibration of the MBT-CBT paleotemperature proxy based on branched tetraether membrane lipids in surface soils. Geochimica et Cosmochimica Acta 96, 215-229.
Prokhorov, I., Kluge, T. and Janssen, C. (2019) Optical clumped isotope thermometry of carbon dioxide. Scientific Reports 9.
Pucéat, E., Joachimski, M.M., Bouilloux, A., Monna, F., Bonin, A., Motreuil, S., Morinière, P., Hénard, S., Mourin, J., Dera, G. and Quesne, D. (2010) Revised phosphate–water fractionation equation reassessing paleotemperatures derived from biogenic apatite. Earth and Planetary Science Letters 298, 135-142.
Rey, C., Collins, B., Goehl, T., Dickson, I.R. and Glimcher, M.J. (1989) The Carbonate Environment in Bone Mineral: A Resolution-Enhanced Fourier Transform Infrared Spectroscopy Study. Calcified Tissue International 45, 157-164.
Rogers, A.K. (2007) Effective hydration temperature of obsedian: a diffusion theory analysis of time-dependent hydration rates. Journal of Archaeological Science 34, 656-665.
Saenger, C., Affek, H.P., Felis, T., Thiagaraian, N., Lough, J.M. and Holcomb, M. (2012) Carbonate clumped isotope variability in shallow water corals: Temperature dependence and growth-related vital effects. Geochimica et Cosmochimica Acta 99, 224-242.
Schauble, E.A., Ghosh, P. and Eiler, J. (2006) Preferential formation of ^{13}C-^{18}O bonds in carbonate minerals, estimated using first-principles lattice dynamics. Geochimica et Cosmochimica Acta 70, 2510-2529.
Smylie, M., Shervette, V. and McDonough, C. (2016) Age, Growth, and Reproduction in Two Coastal Populations of Longnose Gars. Transactions of the American Fisheries Society 145, 1.
Snedden, G.A., Kelso, W.E. and Rutherford, A.D. (1999) Diel and Seasonal Patterns of Spotted Gar Movement and Habitat Use in the Lower Atchafalaya River Basin, Louisiana. Transactions of the American Fisheries Society 128.
Solomon, D.R. (2012) Life history, growth, and genetic diversity of the spotted gar *Lepisosteus oculatus* from peripheral and core populations, Natural Resources and Environment. University of Michigan, p. 171.
Still, C., Powell, R., Aubrecht, D., Kim, Y., Helliker, B., Roberts, D., Richardson, A.D. and Goulden, M. (2019) Thermal imaging in plant and ecosystem ecology: applications and challenges. Ecosphere 10.
Swart, P.K. (2015) The geochemistry of carbonate diagenesis: The past, present, and future. Sedimentology 62, 1233-1304.
Thiagaraian, N., Adkins, J. and Eiler, J. (2011) Carbonate clumped isotope thermometry of deep-sea corals and implications for vital effects. Geochimica et Cosmochimica Acta 75, 4416-4425.
Thomson, K.S. and McCune, A.R. (1984) Scale Structure as Evidence of Growth Patterns in Fossil Semionotid Fishes. Journal of Vertebrate Paleontology 4, 422-429.

Thornton, M.M., Thornton, P.E., Wei, Y., Vose, R.S. and Boyer, A.G. (2017) Daymet: Station-Level Inputs and Model Predicted Values for North America, Version 3. ORNL DAAC, Oak Ridge, Tennessee, USA.
Thornton, P.E., Running, S.W. and White, M.A. (1997) Generating surfaces of daily meteorological variables over large regions of complex terrain. Journal of Hydrology 190, 214-251.
Traverse, A. (2007) Paleopalynology, 2nd ed. Springer, Netherlands.
Tripati, A.K., Eagle, R.A., Thiagarajan, N., Gagnon, A.C., Bauch, H., Halloran, P.R. and Eiler, J.M. (2010) ^{13}C–^{18}O isotope signatures and 'clumped isotope' thermometry in foraminifera and coccoliths. Geochimica et Cosmochimica Acta 74, 5697-5717.
Vennemann, T.W., Hegner, E., Cliff, G. and Benz, G.W. (2001) Isotopic composition of recent shark teeth as a proxy for environmental conditions. Geochimica et Cosmochimica Acta 65, 1583-1599.
Wacker, U., Fiebig, J. and Schoene, B.R. (2013) Clumped isotope analysis of carbonates: comparison of two different acid digestion techniques. Rapid Communications in Mass Spectrometry 27, 1631-1642.
Wacker, U., Rutz, T., Löffler, N., Conrad, A.C., Tütken, T., Böttcher, M.E. and Fiebig, J. (2016) Clumped isotope thermometry of carbonate-bearing apatite: Revised sample pre-treatment, acid digestion, and temperature calibration. Chemical Geology 443, 97-110.
Wang, Z., Schauble, E.A. and Eiler, J.M. (2004) Equilibrium thermodynamics of multiply substituted isotopologues of molecular gases. Geochimica et Cosmochimica Acta 68, 4779 - 4797.
Watkins, J.M., Hunt, J.D., Ryerson, F.J. and DePaolo, D.J. (2014) The influence of temperature, pH, and growth rate on the d18O composition of inorganically precipitated calcite. Earth and Planetary Science Letters 404, 332-343.
Wilf, P. (1997) When are leaves good thermometers? A new case for leaf margin analysis. Paleobiology 23, 373-390.
Wing, S.L. and Greenwood, D.R. (1993) Fossils and Fossil Climate: The case for Equable Continental Interiors in the Eocene. Philosophical Transactions of the Royal Society B 341, 243-252.
Wolfe, J.A. and Spicer, R.A. (1999) Fossil Leaf Character States: Multivariate Analysis, in: Jones, T.P., Rowe, N.P. (Eds.), Fossil Plants and Spores: Modern Techniques. Geological Society, London, pp. 233-239.
Yano, K., Stevens, J.D. and Compagno, L.J.V. (2007) Distribution, reproduction, and feeding of the Greenland shark *Somniosus (Somniosus) microcephalus*, with notes on two other sleeper sharks, *Somniosus (Somniosus) pacificus* and *Somniosus (Somniosus) antarcticus*. Journal of Fish Biology 70, 374-390.
Zaarur, S., Affek, H.P. and Brandon, M.T. (2013) A revised calibration of the clumped isotope thermometer. Earth and Planetary Science Letters 382, 47-57.
Zaarur, S., Olack, G. and Affek, H.P. (2011) Paleo-environmental implication of clumped isotopes in land snail shells. Geochimica et Cosmochimica Acta 75, 6859-6869.

Locality	Coordinates	MAT (°C)	Effective T (°C)	Seasonal Temperatures (°C) (1σ error)			*n*
				AMJ	MJJA	DJF	
Bay Port, MI, USA	43.8569° N, 83.3743° W	9.12 ± 0.22	11.4	14.31 ± 0.29	19.60 ± 0.28	-3.72 ± 0.52	3
North Scott Lake, MI, USA	42.3307° N, 85.9988° W	8.57 ± 0.17	12.9	13.53 ± 0.31	18.61 ± 0.28	-3.25 ± 0.48	2
Rend Lake Dam, IL, USA	38.0371° N, 88.9562° W	13.61 ± 0.19	17.2	19.31 ± 0.22	23.48 ± 0.21	1.67 ± 0.38	1
Ullin, IL, USA	37.2733° N, 89.1838° W	14.21 ± 0.21	16.4	19.10 ± 0.31	23.57 ± 0.32	2.50 ± 0.39	1
Estill Springs, TN, USA	35.2557° N, 86.1332° W	14.87 ± 0.15	17.2	19.43 ± 0.19	23.74 ± 0.22	4.09 ± 0.37	3
Yazoo City, MS, USA	32.8966° N, 90.5419° W	18.41 ± 0.21	20.1	22.78 ± 0.28	26.35 ± 0.29	8.78 ± 0.39	6
Silver Springs, FL, USA	29.1638° N, 82.0777° W	21.73 ± 0.16	22.3	24.33 ± 0.16	26.76 ± 0.08	15.47 ± 0.50	1
Villahermosa, Tabasco, MX	17.9970° N, 92.9280° W	24.81 ± 0.21	26.3	27.08 ± 0.26	27.09 ± 0.25	21.40 ± 0.37	1

Table 1. Seasonal and annual climatic data from NOAA's National Centers for Environmental Information Climate Data Online and Mexico's Servicio Meteorológico Nacional and are averaged for approximately 15 years before the collection date of the gar specimen. AMJ = April May June, MJJA = May June July August, DJF = December January February

Sample	Locality	$\delta^{18}O_{water}$	n	Species	$\delta^{18}O$ (‰ VPBD)	$\delta^{13}C$ (‰ VPBD)	Δ_{47} (Abs. Brand)	Δ_{47} SE
MDF 1	Yazoo City, Mississippi	-3.91	3	*L. osseus*	0.037	--9.357	0.674	0.008
MDF 2			4	*L. osseus*	1.224	--6.759	0.644	0.005
MDF 3			3	*L. osseus*	-0.009	--7.334	0.697	0.006
MDF 4			2	*L. osseus*	-1.993	--9.500	0.645	0.027
MDF 5			3	*L. osseus*	1.765	--7.890	0.673	0.011
MDF 6			3	*L. osseus*	0.666	--7.468	0.680	0.015
					-0.329			
YPM 27686	Estill Springs, Tennessee	-5.68	4	*L. osseus*		--5.966	0.674	0.007
YPM 27692			3	*L. osseus*	-0.494	--6.979	0.710	0.017
YPM 27693			3	*L. osseus*	0.133	-7.066	0.695	0.007
					-3.581			
UMMZ 230705v1	North Scott Lake, Michigan	-7.94	3	*L. oculatus*		-7.682	0.789	0.007
UMMZ 230705v2			2	*L. oculatus*	-5.178	-8.051	0.768	0.007
					-0.370			
UMMZ 180463v1	Bay Port, Michigan	-9.37	3	*L. osseus*		-5.981	0.754	0.015
UMMZ 180463v2			2	*L. osseus*	-6.606	-6.188	0.741	0.011
UMMZ 180463v3			2	*L. osseus*	-2.785	-5.329	0.764	0.046
					6.118			
YPM 27215	Rend Lake Dam, Illinois	-4.13	2	*L. osseus*		-7.716	0.687	0.0002
					-2.777			
IX-03-01	Ullin, Illinois	-4.13	3	*L. osseus*		-6.084	0.726	0.012
					-2.344			
UMMZ 145166	Silver Springs, Florida	-0.84	3	*L. osseus*		-11.311	0.668	0.013
UMMZ 145167			4	*L. osseus*	-1.944	-5.016	0.666	0.028
UMMZ 187727	Tabasco, Mexico	-2.64	3	*A. tropicus*	4.595	-6.768	0.661	0.002

Table 2. Data for all samples. Δ_{47} values are given in the absolute reference frame as outlined in Dennis et al. (2011). ^{17}O is corrected using the Brand et al. (2010) parameters. Abbreviations are YPM for the Yale Peabody Museum, UMMZ for the University of Michigan Museum of Zoology, and MDF for Mississippi Department of Wildlife, Fisheries, and Parks.

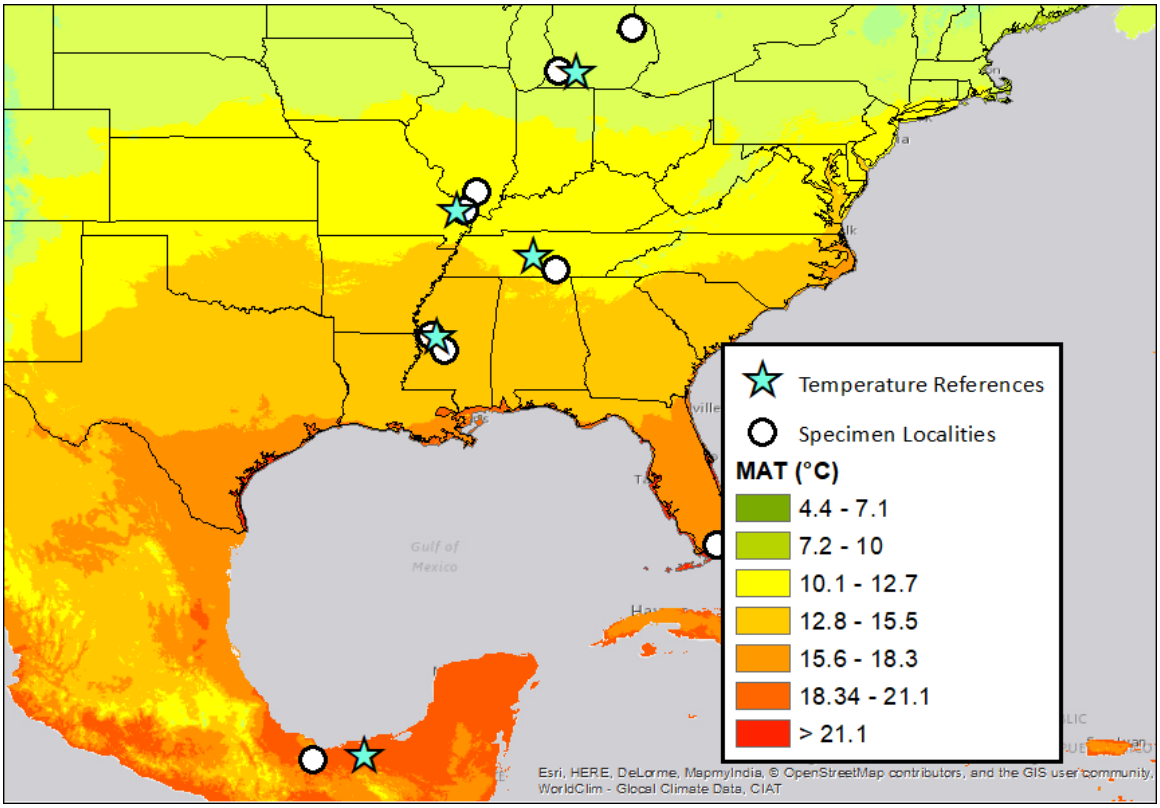

Figure 1. Map of specimen localities (white circles) and the closest weather station (light blue stars) for temperature data in table 1 (National Oceanic & Atmospheric Administration, National Environmental Satellite, Data, and Information Science) superimposed on MAT (WorldClim Global Climate Data). Although gars do not migrate, specimens were preferentially chosen from dams or reservoirs or small streams to minimize temperature fluctuations.

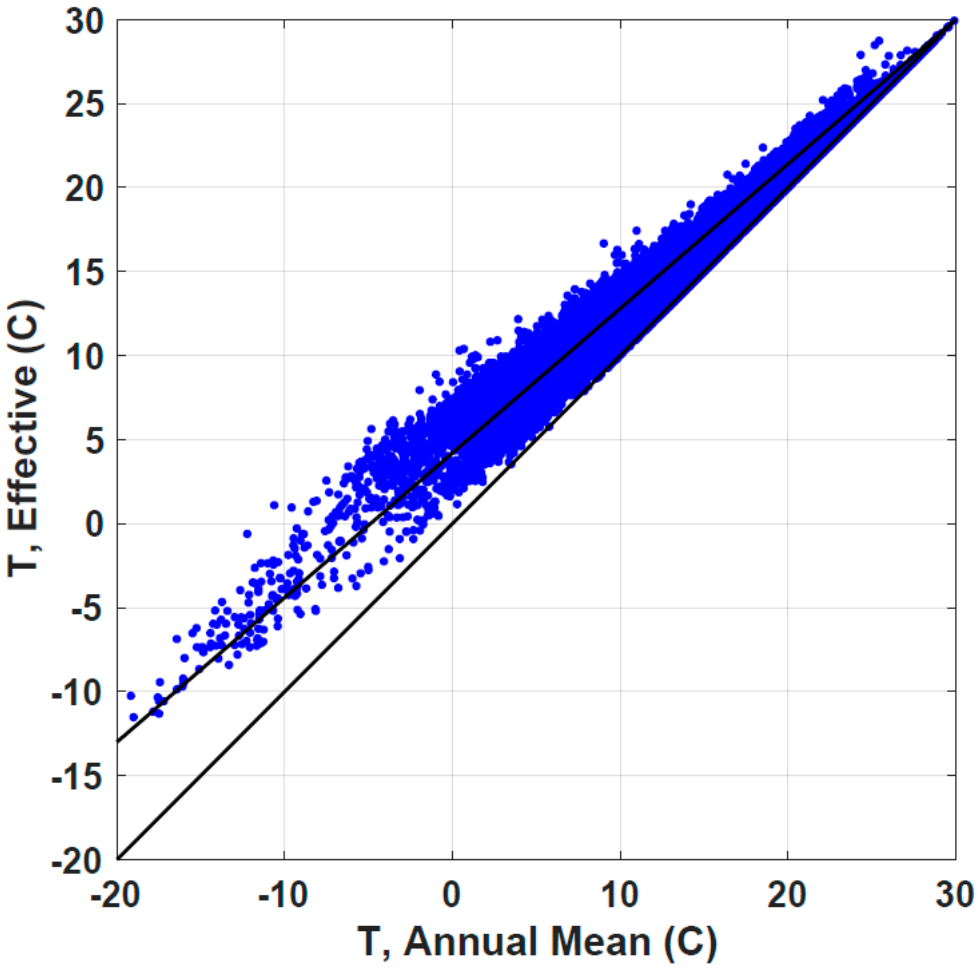

Figure 2. Comparison of $T_{effective}$ against MAT (°C) for 19,874 North America stations (excluding Greenland) for the time interval from 1900 to 2018.

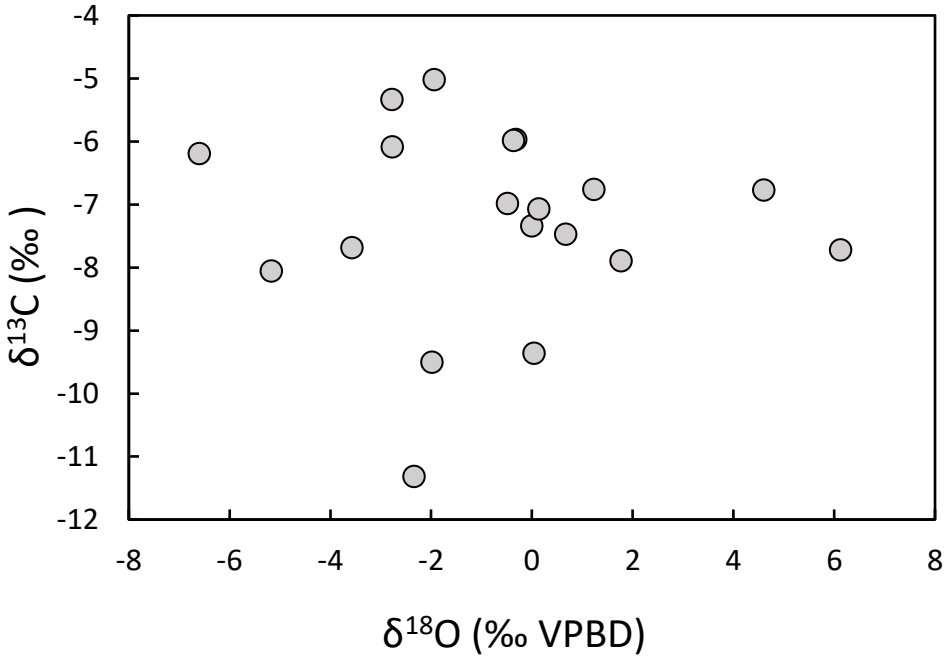

Figure 3. Comparison between $\delta^{18}O$ (VPBD) and $\delta^{13}C$. There is no correlation between $\delta^{18}O$ and $\delta^{13}C$.

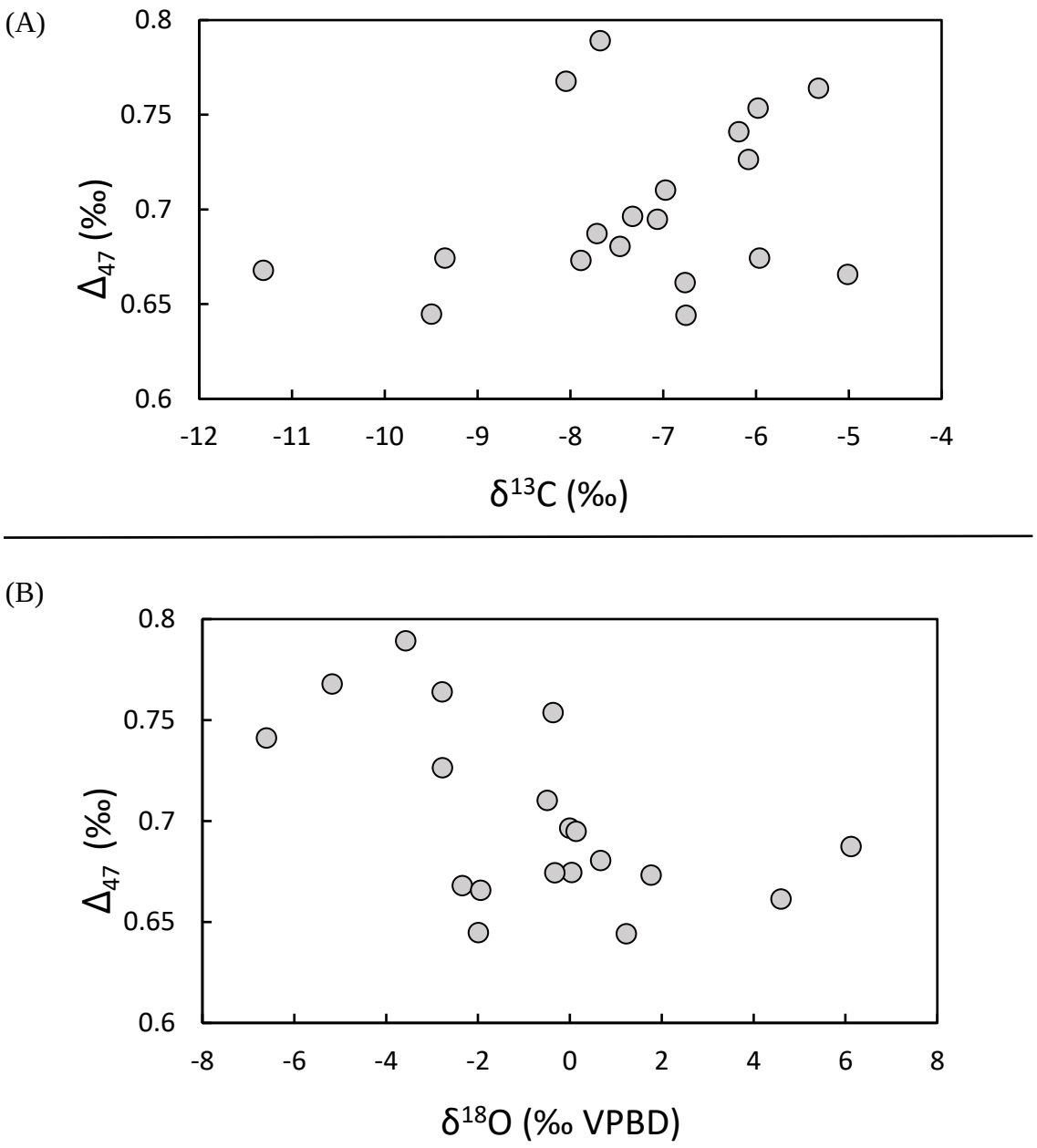

Figure 4. Comparison between Δ_{47} and $\delta^{13}C$ (A) and Δ_{47} and $\delta^{18}O$ (VPBD) in gar scales (B). There is no correlation between $\delta^{18}O$ or $\delta^{13}C$ and Δ_{47}. Δ_{47} is independent of the bulk composition.

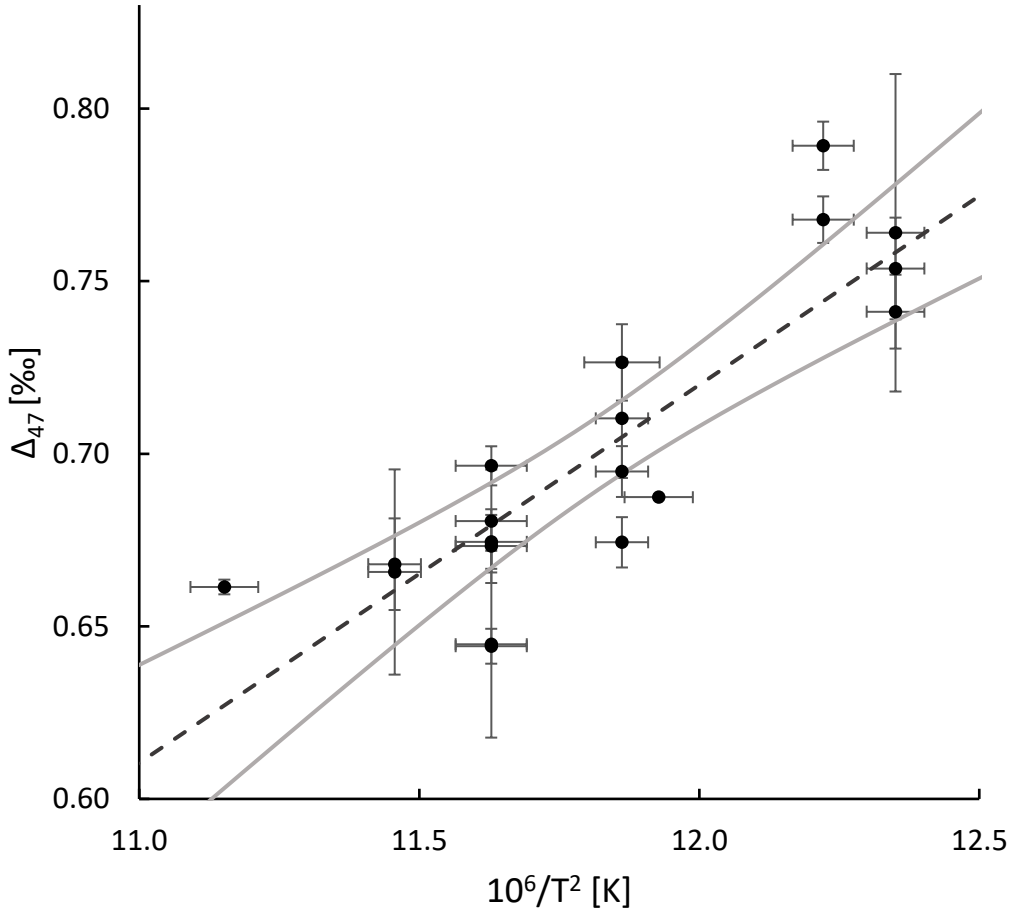

Figure 5. Empirical relationship between Δ_{47} in gar scales and temperature (K). Error bars are 1 SE.

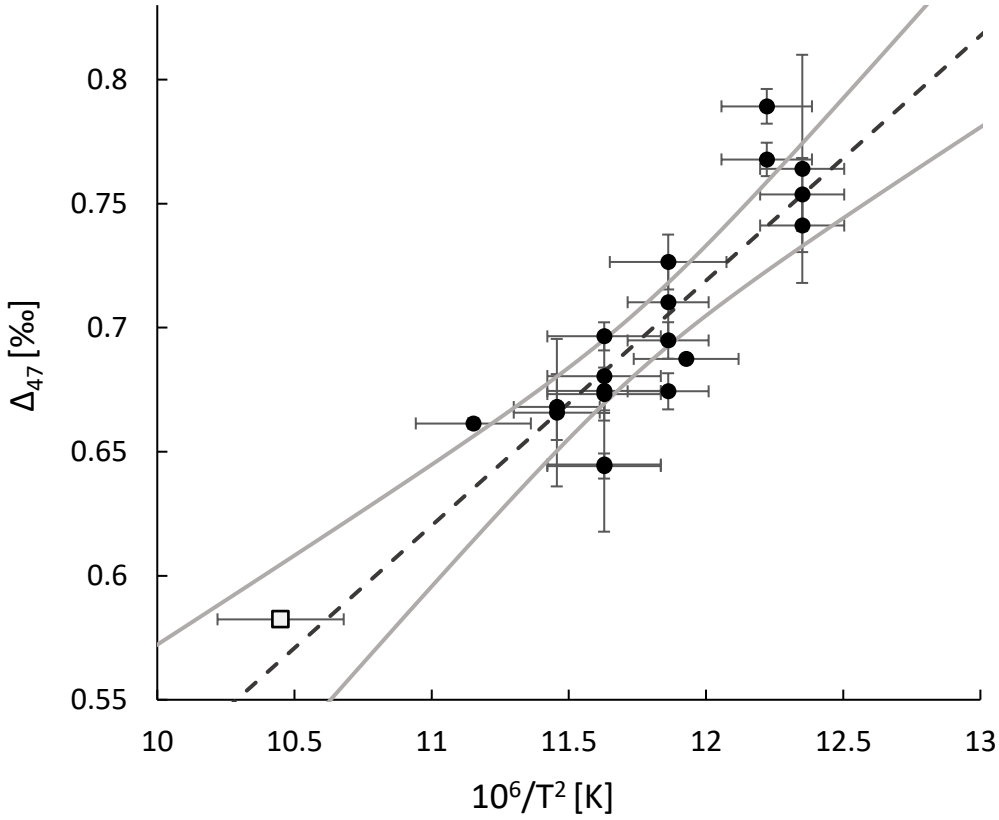

Figure 6. Empirical relationship between Δ_{47} in biogenic apatite, including gar scales, and temperature (K). White open circle is elephant enamel from Löffler et al. (2019).